ChemComm

Accepted Manuscript

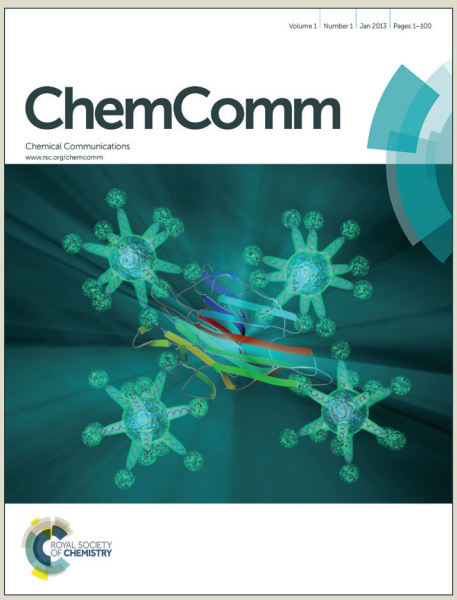

ROYAL SOCIETY OF CHEMISTRY

www.rsc.org/chemcomm

Cite this: DOI: 10.1039/c0xx00000x

www.rsc.org/xxxxxx

ARTICLE TYPE

Structure optimization of prussian blue analogue cathode materials for advanced sodium ion batteries

Dezhi Yang,[a] Jing Xu,[a] Xiao-Zhen Liao,*[a] Yu-Shi He,[a] Haimei Liu[b] and Zi-Feng Ma*[a]

Received (in XXX, XXX) Xth XXXXXXXXX 20XX, Accepted Xth XXXXXXXXX 20XX

DOI: 10.1039/b000000x

A structure optimized prussian blue analogue $Na_{1.76}Ni_{0.12}Mn_{0.88}[Fe(CN)_6]_{0.98}$ (PBMN) is synthesized and investigated. Coexistence of inactive Ni^{2+} (Fe-C≡N-Ni group) with active $Mn^{2+/3+}$ (Fe-C≡N-Mn group) balances the structure disturbances caused by the redox reactions. This cathode material exhibits particularly excellent cycle life with high capacity (118.2 mAh/g).

Low cost, long life time and highly efficient energy storage systems have attracted great attentions for their applications in the electric grids and electric vehicles (EVs). Lithium ion batteries (LIBs) are supposed to be appropriate energy storage devices. [1-3] However, with the increasing demand of large-scale energy storage systems, the cost of LIBs and the limitation of lithium mineral resources appear to restrain the huge applications of LIBs. Sodium is the 4th most abundant element on the earth with lower cost than lithium. Batteries based on sodium ion such as Na/S and $Na/NiCl_2$ have been developed but with high operating temperature (300 to 350℃) that bring about increased cost. Thus, room-temperature rechargeable sodium ion batteries (SIBs) are highly concerned and motivating large advances in developing various electrode materials.[4-9]

Recently, Prussian blue and its analogues (PBAs) attract great interest and have been investigated as cathode materials for SIBs.[10,11] Most of PBAs exhibit an open and zeolite-like structure composing of a cubic framework of transition metal cations bounded by hexacynometallate groups, and allow alkali cations (Na^+, Li^+, K^+) to insert/extract rapidly through their wide channels. Typically, the zeolite water and alkali cations (A^+) locate in the nanopores of the host framework. Some PBAs also have ligand water locating at the $Fe(CN)_6$ vacancies and coordinating to transition metal cations, which is indicated as hole-doped structure.[10-13] The $Fe(CN)_6$ vacancies and water will deteriorate the electrochemical performances of PBAs in SIBs.[14] The PBAs such as $Na_2FeFe(CN)_6$ (PBF), $Na_2CuFe(CN)_6$ (PBC) and $Na_2MnFe(CN)_6$ (PBM) have two redox active sites of M (transition metal cations, eg. Fe^{2+}, Cu^{2+}, Mn^{2+}) and $Fe(CN)_6^{4-}$, and can deliver specific capacities of more than 100 mAh/g. When the Fe sites of $Fe(CN)_6^{4-}$ group are reduced/oxidized, the lattice constants remain nearly unchanged. However, the lattice constants would increase or decrease in small ranges accompanying with redox reaction of M sites during charge/discharge, [10-18] which may cause the Fe-C≡N-M bridges to collapse more easily especially for hole-doped PBAs, then result in decreased cycle life for SIBs. On the other hand, the $Na_2NiFe(CN)_6$ (PBN) sample has only one redox active site of $Fe(CN)_6^{4-}$ in its structure. Therefore, the SIBs with PBN as cathode show excellent cycle properties but low specific capacities.[12,19] Nevertheless, the practical application of PBAs in SIBs requires high capacity as well as long cycle life.

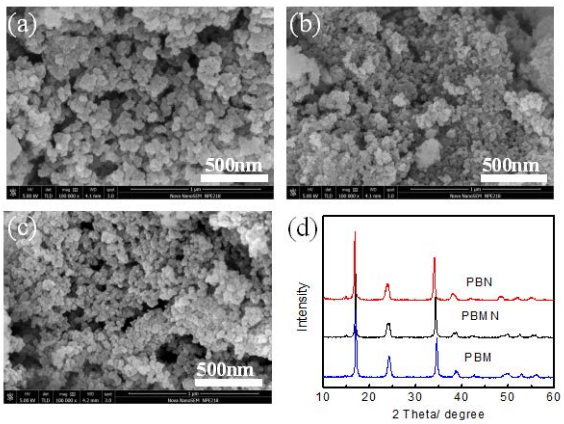

Fig.1 SEM images of the prepared PBM (a), PBN (b) and PBMN (c) samples; (d): X-ray diffraction patterns of the PBM, PBN and PBMN samples.

In this work, based on PBM and PBN, we designed a high performance $Na_2Ni_xMn_yFe(CN)_6$ (PBMN) cathode material by substituting electrochemical inert Ni sites for part of Mn redox sites. The PBM, PBN and $Na_2Ni_xMn_yFe(CN)_6$ (PBMN) with low $Fe(CN)_6$ vacancies were synthesized by mixing precursor solutions drop by drop and analyzed via elemental analysis and inductively coupled plasma (ICP) analysis (See S1 of ESI). The chemical composition of the PBM, PBN and PBMN were revealed to be $Na_{1.8}Mn[Fe(CN)_6]_{0.99}*□_{0.01}$ (□=$Fe(CN)_6$ vacancy), $Na_{1.86}Ni[Fe(CN)_6]_{0.96}*□_{0.04}$ and $Na_{1.76}Ni_{0.12}Mn_{0.88}[Fe(CN)_6]_{0.98}*□_{0.02}$, respectively. Fig.1 shows SEM images of the prepared PBM (a), PBN (b) and PBMN (c) samples. It reveals that the nanoparticles of PBM, PBN and PBMN have average diameters of ca. 20–50nm. These small diameters decreased the diffusion distance of Na^+ in the crystal framework. From the results of thermo gravimetric analysis (TG) (See S2 of ESI), the water contents of PBM, PBN and PBMN were 12.7%, 11.7% and 12.4%, respectively.

Fig.1d shows the XRD patterns of PBM, PBN and PBMN samples. The diffraction patterns can be indexed to the face-centred cubic structure (Space group Fm3m) as reported before.[18,19] The diffraction peaks are sharp and strong, indicating that these samples have high crystallinity. The atomic radius of Mn is almost equal to the atomic radius of Ni. Thus, when the Ni element replacing the Mn element in the prussian blue structure, the cubic framework is still in good order. The lattice parameters of PBM, PBN and PBMN are calculated to be 10.26 Å, 10.47 Å and 10.32 Å, respectively. As shown in the structure schematic of PBMN where Ni elements have replaced part of Mn elements successfully (See S3 of ESI), the Fe^{2+} ions are octahedrally coordinated to the carbon ends of the CN group while the M ions (Mn^{2+} or Ni^{2+}) to the nitrogen ends. The inner space in the cubic cell is large enough to allow rapid insertion/extraction of Na^+ without obvious disturbance of the crystal framework. Since all samples were synthesized under dark environment, the $Fe(CN)_6^{4-}$ group kept stable rather than oxidized to $Fe(CN)_6^{3-}$ group or decomposed. Hence, the signal of trivalent iron was unconspicuous in the XPS spectra of PBMN (See S4 of ESI). The Ni in the PBMN was detected to be bivalence. But the Mn was sensed to be multi-valence. It is known that Mn element has six stable oxidation states, three oxidation states show significant multiple splitting. These multiple splitting structures present overlapped binding energy ranges, thus cause serious challenge for both qualitative and quantitative analyses. [20, 21] Calculated from the chemical formula of PBMN, the average valance of Mn is +2.18.

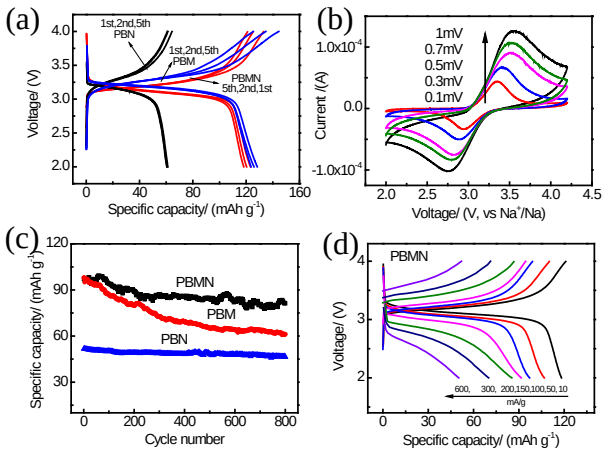

Fig.2 (a): The galvanostatic charge–discharge profiles of PBM, PBN and PBMN between 2.0V-4.0V at 10 mA/g. (b): Cyclic voltammograms of PBMN at different scan rate between 2V and 4.2V. (c): Cyclic performances of PBM, PBN and PBMN between 2.0V-4.0V at 100 mA g^{-1}. (d): The galvanostatic charge–discharge curves of PBMN at different rates.

The electrochemical performances of the PBM, PBN and PBMN as cathode materials for SIBs are directly related to their crystal structures. Fig.2a shows charge/discharge curves of PBM, PBN and PBMN between 2.0V-4.0V at 10 mA/g. The discharge voltage plateaus of all the samples lie between 3.3V and 3V, and the first discharge capapcities were 62.2 mAh/g, 128.4 mAh/g and 123.3 mAh/g for PBN, PBM and PBMN, respectively. The first charge/discharge coulombic efficiency of PBM, PBN and PBMN reached 88.86%, 93.25% and 92.71%, respectively. From the second cycle, their coulombic efficiencies increased and achieved a stable value of above 98% after five cycles that confirmed the stable frameworks for Na^+ insertion/extraction.

The charge/discharge capacity is decided by the redox sites in the crystal framework. The PBM sample had two redox sites of Mn ion and $Fe(CN)_6$ group to deliver a capacity of about 123.7 mAh/g. The PBN only demonstrated a capacity of about 61.2 mAh/g due to only one redox site of $Fe(CN)_6$ group in the framework. While in the PBMN framework, part of Mn sites were replaced by Ni, thus delivered a lower capacity of 118.2 mAh/g. However, compared with the theoretical capacity of PBMN (164 mAh/g) that calculated from full redox reactions of $Fe(CN)_6$ and feasible Mn sites, the real discharged capacity of PBMN still needs to be improved. In other words, only part of redox sites in the PB structure responded to charge/discharge of Na^+. That is why the discharged capacity of PBMN was still close to PBM. Fig.2b shows the cyclic voltammetry (CV) curves of PBMN. One pair of redox peaks is observed, which is consistent with the one plateau discharge voltage profiles of PBMN. This phenomenon indicated that the Mn^{2+}/Mn^{3+} couple had comparable energies with the $Fe(CN)_6^{4-}/Fe(CN)_6^{3-}$ in the PBMN.[18]

The cycle life time is important to evaluate the performances of SIBs. Fig.2c shows the cycle stability of the PBM, PBN and PBMN at 100 mA/g. Although the PBM, PBN and PBMN were synthesized carefully, there were still some $Fe(CN)_6$ vacancies in their framework, which caused the crystal structure becoming more sensitive to tiny structure disturbances. During insertion/extraction of Na^+, the lattice constants remained unchanged when the $Fe(CN)_6^{4-}/Fe(CN)_6^{3-}$ group were reduced/oxidized, but were changed when the redox reaction of Mn^{2+}/Mn^{3+} happened. Therefore, the capacity retention of PBM decreased to 63.4% after 800 cycles. On the other hand, the PBN kept capacity retention of 89.5%. Importantly, the capacity retention of PBMN reached as high as 83.8%. The Ni sites in the PBMN framework are electrochemical inertness and thus are able to balance the structure disturbances caused by the redox reaction of Mn^{2+}/Mn^{3+}. In the SEM image and XRD result of PBMN electrode after 800 charge/discharge cycles (See S5 and S6 of ESI), no obvious change was detected, which was consistent with its excellent cycle performance. The XRD pattern of the electrode after 800 cycles still presents the main peaks of PBMN strongly, indicating the inner crystal structure was still in good order. The PBMNs with different Ni content were also investigated (See S7 of ESI). With increased Ni content in the PBMN, the discharge capacity was significantly decreased but the cycle stability was increased in small ranges. In other words, $Na_{1.76}Ni_{0.12}Mn_{0.88}Fe(CN)_6$ with low Ni content was more appropriate for sodium ion batteries. Fig.2d shows the rate performance of PBMN at various current densities. The PBMN exhibited a capacity of 50.2 mAh/g even under high current density of 600 mA/g, which indicated fast insertion/extraction kinetics of Na^+ in the PBMN framework.

As discussed above, the PBMN electrode was verified to perform excellent cycle life with high capacity. Thus, we applied this qualified cathode material to fabricate and characterize an advanced sodium ion battery (ASIB). Commercial hard carbon was applied as anode material in this ASIB. As shown in its

initial and second charge/discharge curves from 0.05V to 2.0V under 25 mA/g (See S8 of ESI), the hard carbon delivered a capacity of 240.3 mAh/g corresponding to the extraction of Na^+ in the first cycle, which is accorded with reported results.[22] After 200 cycles, the capacity of hard carbon decreased to 195.5 mAh/g but the coulombic efficiency maintained about 99.9% stably through the measurement.

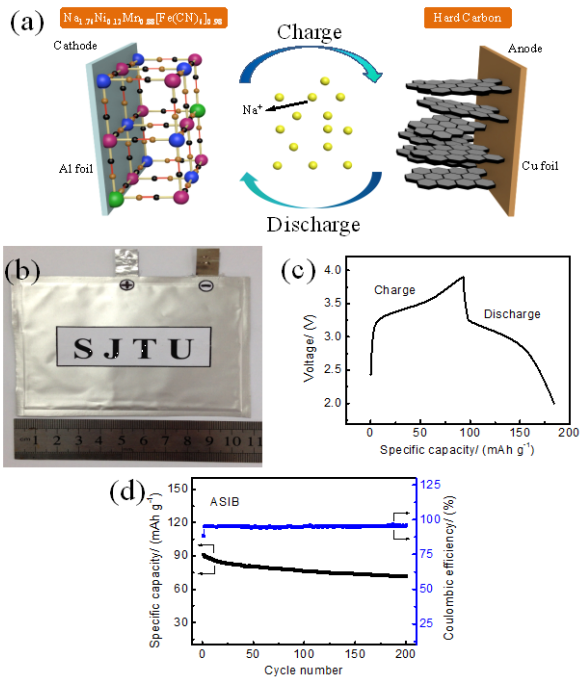

Fig.3 (a): The schematic of ASIB. (b): The photograph of ASIB. (c): The charge–discharge curves, and (d): the cycle performances and the coulombic efficiencies of ASIB between 2V-3.9V at 100 mA/g.

Fig.3a&b shows the schematic structure and photograph of the prepared ASIB. Compared with coin cell, this ASIB was packaged by aluminium plastic film and much similar to commercial soft-packing battery. As far as we know, this soft-packing sodium ion battery was first reported. A high capacity of 90.8 mAh/g (based on cathode mass) was delivered under 100 mA/g, as shown in Fig.3c. The coulombic efficiency reaches about 88.2% in the first cycle, then increased to 95% in the subsequent cycles. Assuming that 30% by weight loading of the cathode active materials is possible in a commercial full cell, the energy density and the power density are estimated to be 81.72 Wh/kg and 90 W/kg, respectively, which can compete with the lead-acid batteries (about 40 Wh/kg). Fig.3d shows the cycle performance and the coulombic efficiencies of the prepared ASIB. It can be clearly seen that the discharge capacity still remains 71.62 mAh/g even after 200 cycles. As seen in Fig. 2 (c), the capacity retention of PBMN reaches about 91.67% after 200 cycles. But the capacity retention of hard carbon only reaches 81.36% after 200 cycles (See S8 of ESI). The PBMN cathode exhibited better cycling stability than that of the hard carbon anode. Thus, the decreased capacity might due to the limit of the cycle property of hard carbon. Developing advanced anode materials, adding featured additives to the electrolyte and designing special membrane will accelerate the practical applications of PBMN in the commercial soft-packing sodium ion batteries.

In summary, we synthesized the PBMN cathode material and applied it to SIBs successfully. In the framework of PBMN, the Ni and Mn both existed and still remained the original cubic structure of prussian blue well. During insertion/extraction of Na^+, the Ni sites were unreactive and could balance the tiny structure disturbances caused by the redox reactions of Mn sites. Thus, the PBMN electrode delivered a high capacity of 118.2 mAh/g (10 mA/g) as well as good rate capability, and also exhibited particularly excellent cycle stability with 83.8% capacity retention after 800 cycles (100 mA/g) . In order to verify the practical application of PBMN in the commercial soft-packing sodium ion batteries, the PBMN cathode and hard carbon anode were assembled together and packaged by aluminium plastic film to work as a full cell. The cell delivered an energy density of 81.72 Wh/kg and a power density of 90 W/kg under 100 mA/g that could compete with the lead-acid batteries. The cell also showed an excellent cycle life of over 200 cycles with capacity retention of 79%. Hence, this work provides a promising method to enhance the cyclic performances of PBA cathode materials for SIBs. A full soft-packing sodium ion battery was also fabricated to demonstrate that the PBMN cathode material is highly feasible choice for the commercial application.

The authors are grateful for the financial support of this work by the Natural Science Foundation of China (21336003 and 21073120), and the Major Basic Research Program of China (2014CB239700).

Notes and references

[a] *Institute of Electrochemical and Energy Technology, Department of Chemical Engineering, Shanghai Jiao Tong University, Shanghai 200240, China. Fax: +86 21 5474 1297; Tel: +86 21 5474 2894; E-mail: zfma@sjtu.edu.cn; liaoxz@sjtu.edu.cn*

[b] *College of Environmental and Chemical Engineering, Shanghai University of Electric Power, Shanghai 200090, China*

† Electronic Supplementary Information (ESI) available: [details of any supplementary information available should be included here]. See DOI: 10.1039/b000000x/

1. B. Dunn, H. Kamath, J. M. Tarascon, *Science*, 2011, **334**, 928.
2. Z. G. Yang, J. L. Zhang, M. C. W. Kintner-Meyer, X. C. Lu, D. W. Choi, J. P. Lemmon, J. Liu, *Chem. Rev.*, 2011, **111**, 3577.
3. J. B. Goodenough , Y. Kim , *Chem. Mater.*, 2010, **22**, 587 .
4. J. Liu, J.G. Zhang, Z. G.Yang, J. P. Lemmon, C. Imhoff, G. L. Graff, L. Y. Li, J. Z. Hu, C. M. Wang, J. Xiao, G. Xia, V. V. Viswanathan, S. Baskaran, V. Sprenkle, X. L. Li, Y. Y. Shao, B. Schwenzer, *Adv. Funct Mater.*, 2013, **23**, 929.
5. H. Pan, Y.-S. Hu, L. Chen, *Energy Environ. Sci.*, 2013, **6**, 2338.
6. V. Palomaresa, P. Serras, I. Villaluenga, K. B. Hueso, J. Carretero-González, T. Rojo, *Energy Environ. Sci.*, 2012, **5**, 5884.
7. D. Yang, X.-Z. Liao, B. Huang, J. Shen, Y.-S. He, Z.-F. Ma, *J. Mater. Chem. A*, 2013, **1**, 13417.
8. D. Yang, X.-Z. Liao, J. Shen, Y.-S. He, Z.-F. Ma, *J. Mater. Chem. A*, 2014, **2**, 6723.
9. K. B. Hueso, M. Armand, T. Rojo, *Energy Environ. Sci,.* 2013, **6**, 734.
10. Y. Lu, L. Wang, J. Cheng, J. B. Goodenough, *Chem. Commun.*, 2012, **48**, 6544.
11. C. D. Wessells, R. A. Huggins, Y. Cui, *Nat. Commun.*, 2011, **2**, 550.
12. Y. Moritomo, M. Takachi, Y. Kurihara, T. Matsuda, *Advances in Materials Science and Engineering*, 2013, **2013**, 17.
13. T. Matsuda, J. E. Kim, K. Ohoyama, Y. Moritomo, *Phys. Rev. B*, 2009, **79**, 172302.

14. Y. You, X.-L. Wu, Y.-X. Yin, Y.-G. Guo, *Energy Environ. Sci.*, 2014, **7**, 1643.
15. Y. Yue, A. J. Binder, B. Guo, Z. Zhang, Z.-A. Qiao, C. Tian, S. Dai, *Angew. Chem.*, 2014, **126**, 3198.
16. Y. Mizuno, M. Okubo, E. Hosono, T. Kudo, H. Zhou, K. Oh-ishi, *J. Phys. Chem. C*, 2013, **117**, 10877.
17. S.-H. Yu, M. Shokouhimehr, T. Hyeon, Y.-E. Sung, *ECS Electrochem. Lett.*, 2013, **2**, A39.
18 L. Wang, Y. Lu, J. Liu, M. Xu, J. Cheng, D. Zhang, J. B. Goodenough, *Angew. Chem. Int. Ed.*, 2013, **52**, 1964.
19. X. Wu, Y. Cao, X. Ai, J. Qian, H. Yang, *Electrochem. Commun.*, 2013, **31**, 145.
20. M. C. Biesinger, B. P. Payne, A. P. Grosvenor, L.W.M. Lau, A. R. Gerson, R. St.C. Smart, *Appl. Surf. Sci.*, 2011, **257**, 2717.
21. Y. Wang, H. Zhong, L. Hu, N. Yan, H. Hu, Q. Chen, *J. Mater. Chem. A*, 2013, **1**, 2621.
22. S. Komaba, W. Murata, T. Ishikawa, N. Yabuuchi, T. Ozeki, T. Nakayama, A. Ogata, K. Gotoh, K. Fujiwara, *Adv. Funct. Mater.*, 2011, **21**, 3859.